Universal Parametric Geometry Representation Method

Brenda M. Kulfan*

Boeing Commercial Airplane Group, Seattle, Washington 98124

For aerodynamic design optimization, it is very desirable to limit the number of the geometric design variables. In this paper, a "fundamental" parametric airfoil geometry representation method is presented. The method includes the introduction of a geometric "class function/shape function" transformation technique, such that round-nose/ sharp aft-end geometries, as well as other classes of geometries, can be represented exactly by analytic well-behaved and simple mathematical functions having easily observed physical features. The fundamental parametric geometry representation method is shown to describe an essentially limitless design space composed entirely of analytically smooth geometries. The class function/shape function methodology is then extended to more general three-dimensional applications such as wing, body, ducts, and nacelles. It is shown that a general three-dimensional geometry can be represented by a distribution of fundamental shapes, and that the class function/shape function methodology can be used to describe the fundamental shapes as well as the distributions of the fundamental shapes. With this very robust, versatile, and simple method, a three-dimensional geometry is defined in a design space by the distribution of class functions and the shape functions. This design space geometry is then transformed into the physical space in which the actual geometry definition is obtained. A number of applications of the class function/ shape function transformation method to nacelles, ducts, wings, and bodies are presented to illustrate the versatility of this new methodology. It is shown that relatively few numbers of variables are required to represent arbitrary three-dimensional geometries such as an aircraft wing, nacelle, or body.

I. Introduction

T HE choice of the mathematical representations of the geometry of an aircraft or aircraft component that is used in any particular aerodynamic design optimization process, along with the selection of the type of optimization algorithm, have a profound effect on such things as the computational time and resources, the extent and general nature of the design space, and whether or not the geometries contained in the design space are smooth or irregular, or even physically realistic or acceptable.

The method of geometry representation also affects the suitability of the selected optimization process. For example, the use of discrete coordinates as design variables may not be suitable for use with a genetic optimization process because the resulting design space could be heavily populated with geometries having bumpy irregular surfaces, thus making the possibility of locating an optimum smooth surface practically impossible. The geometry representation method also affects whether a meaningful "optimum" is contained in the design space and if an optimum design exists, whether or not it can be found.

Desirable characteristics for any geometric representation technique include: 1) well behaved and produces smooth and realistic shapes; 2) mathematically efficient and numerically stable process that is fast, accurate, and consistent; 3) requires relatively few variables to represent a large enough design space to contain optimum aerodynamic shapes for a variety of design conditions and constraints; 4) allows specification of design parameters such as leading-edge radius, boat-tail angle, airfoil closure; 5) provides easy control for designing and editing the shape of a curve; 6) intuitive–geometry algorithm that has an intuitive and geometric interpretation.

The geometric definition of any aircraft consists of representing the basic defining components of the configuration by using two fundamental types of shapes [1] together with the distribution of the shapes along each of the components. The two fundamental defining shapes include the following:

Class 1: Wing-airfoil-type shapes for defining such components as 1) airfoils/wings; 2) helicopter rotors, turbomachinery blades; 3) horizontal and vertical tails, canards, winglets, struts; and 4) bodies or nacelles of revolution.

Class 2: Body cross-section-type shapes for defining such components as 1) aircraft fuselages (cross sections); 2) rotor hubs and shrouds; 3) channels, ducts, and tubing; and 4) lifting bodies.

The mathematical description of class 1 geometries having a round nose and pointed aft end is a continuous but nonanalytic function because of the infinite slope at the nose and the corresponding large variations of curvature over the surface. Similarly, in the conventional Cartesian coordinate system, the mathematical definitions of the cross sections of class 2 type of geometries are generally also a continuous but nonanalytic function.

Consequently, a large number of coordinates are typically required to describe either class 1 or class 2 types of geometries. Numerous methods [2–8] have been devised to numerically represent class 1 airfoil type geometries for use in aerodynamic design, optimization, and parametric studies. Commonly used geometry representation methods typically fail to meet the complete set of the previously defined desirable features [9].

A previous paper [9] focused on the class 1 type of two-dimensional airfoil shapes that have a round nose and a pointed aft end. A new and powerful methodology for describing such airfoil type geometries was presented. The method was shown to apply equally well to axisymmetric nacelles and bodies of revolution. In the current paper [10], the methodology is extended to represent class 2 geometries as well as general three-dimensional geometries.

A brief description and review of the initial developments of the methodology will be shown, because knowledge of this information is essential to the understanding of the extension of the methodology that is presented in the present paper. The concept of representing arbitrary three-dimensional geometries as a distribution of fundamental shapes is then discussed. It is shown that the previous

*Engineer/Scientist–Technical Fellow, Enabling Technology & Research, Post Office Box 3707, Mail Stop 67-LF. AIAA Member.

method developed for two-dimensional airfoils and axisymmetric bodies or nacelles can be used to mathematically describe the fundamental shapes, as well as the distribution of the shapes for defining rather arbitrary three-dimensional geometries. Applications of the extended methodology to a variety of three-dimensional geometries including wings and nacelles are shown.

II. Mathematical Description of Airfoil Geometry

Although the discussion that follows specifically focuses on two-dimensional airfoils, all of the results and conclusions apply equally to both axisymmetric nacelles and bodies of revolution.

In the case of the round-nose airfoil described in a fixed Cartesian coordinate system, the slopes and second derivatives of the surface geometry are infinite at the nose, and large changes in curvature occur over the entire airfoil surface. The mathematical characteristics of the airfoil surfaces are therefore nonanalytic functions with singularities in all derivatives at the nose.

The approach used in [9] to develop an improved airfoil geometry representation method was based on a technique that the author has often used successfully in the past, to develop effective computational methods to deal with numerically difficult functions. The technique that was used to develop an efficient well-behaved method to geometrically describe such geometry involved the following steps:

1) Develop a general mathematical equation necessary and sufficient to describe the geometry of any round-nose/sharp aft-end airfoil.

2) Examine the general nature of this mathematical expression to determine the elements of the mathematical expression that are the source of the numerical singularity.

3) Rearrange or transform the parts of the mathematical expression to eliminate the numerical singularity.

4) This resulted in identifying and defining a "shape function" transformation technique such that the definition of an airfoil using this shape function becomes a simple well-behaved analytic function with easily controlled key physical design features.

5) Subsequently, a "class function" was introduced to generalize the methodology for applications to a wide variety of fundamental two-dimensional airfoils and axisymmetric nacelle and body geometries.

A summary of this approach is discussed next.

The general and necessary form of the mathematical expression that represents the typical airfoil geometry [9,10] is

$$\zeta(\psi) = \sqrt{\psi}(1 - \psi) \sum_{i=0}^{N} A_i \psi^i + \psi \zeta_T \qquad (1)$$

where $\psi = x/c$, $\zeta = z/c$, and $\zeta_T = \Delta Z_{TE}/c$. The term $\sqrt{\psi}$ is the only mathematical function that will provide a round nose. The term $(1 - \psi)$ is required to ensure a sharp trailing edge. The term $\psi \zeta_T$ provides control of the trailing-edge thickness. The term

$$\sum_{i=0}^{\infty} A_i \psi^i$$

represents a general function that describes the unique shape of the geometry between the round nose and the sharp aft end.

This term is shown for convenience as a power series but it can be represented by any appropriate well-behaved analytic mathematical function.

III. Airfoil Shape Function

The source of the nonanalytic characteristic of the basic airfoil equation is associated with the square root term in Eq. (1).

Let us define the shape function $S(\psi)$ which is derived from the basic geometry equation by first subtracting the airfoil trailing-edge thickness term and then dividing by the round-nose and sharp-end terms.

This gives

$$S(\psi) \equiv \frac{\zeta(\psi) - \psi \xi_T}{\sqrt{\psi}[1 - \psi]} \qquad (2)$$

The equation that represents the S function, which is obtained from Eqs. (1) and (2), becomes the rather simple expression

$$S(\psi) = \sum_{i=0}^{N} [A_i \psi^i] \qquad (3)$$

The shape function equation is a simple well-behaved analytic equation for which the "eye" is well adapted to see the represented detailed features of an airfoil and to make critical comparisons between various geometries.

It was shown in [9] that the nose radius, the trailing-edge thickness, and the boat-tail angle are directly related to the unique bounding values of the $S(\psi)$ function. The value of the shape function at $x/c = 0$ is directly related to the airfoil leading-edge nose radius R_{LE} and the airfoil chord length C by the relation

$$S(0) = \sqrt{2[R_{LE}/C]} \qquad (4)$$

The value of the shape function at $x/c = 1$ is directly related to the airfoil boat-tail angle β and trailing-edge thickness by the relation

$$S(1) = \tan \beta + \frac{\Delta z_{TE}}{c} \qquad (5)$$

Hence, in the transformed coordinate system, specifying the endpoints of the shape function provides an easy way to define and to control the leading-edge radius, the closure boat-tail angle, and trailing-edge thickness.

An example of the transformation of the actual airfoil geometry to the corresponding shape function is shown in Fig. 1. The transformation of the constant Z_{max} height line, and the constant boat-tail angle line, are also shown as curves in the transformed plane.

The shape function for this example airfoil is seen to be approximately a straight line with the value at zero related to the leading-edge radius of curvature and the value at the aft end equal to tangent of the boat-tail angle plus the ratio of trailing-edge thickness/chord length. It is readily apparent that the shape function is indeed a very simple analytic function.

The areas of the airfoil that affect its drag and performance characteristics of the airfoil are readily visible on the shape function curve as shown in the figure. Furthermore, the shape function provides easy control of the airfoil critical design parameters.

The term $\sqrt{\psi}[1 - \psi]$ will be defined the class function $C(\psi)$ with the general mathematical form

$$C_{N2}^{N1}(\psi) \triangleq (\psi)^{N1}[1 - \psi]^{N2} \qquad (6)$$

For a round-nose airfoil $N1 = 0.5$ and $N2 = 1.0$.

In [9], it was shown that different combinations of the exponents in the class function, together with a unit shape function, mathematically defines a variety of basic general classes of geometric shapes:

$$N1 = 0.5 \text{ and } N2 = 1.0$$

define a NACA-type round nose and pointed aft end airfoil.

$$N1 = 0.5 \text{ and } N2 = 0.5$$

define an elliptic airfoil or an ellipsoid body of revolution.

$$N1 = 1.0 \text{ and } N2 = 1.0$$

define a biconvex airfoil or an ogive body. The biconvex airfoil is the minimum drag supersonic airfoil for a given area.
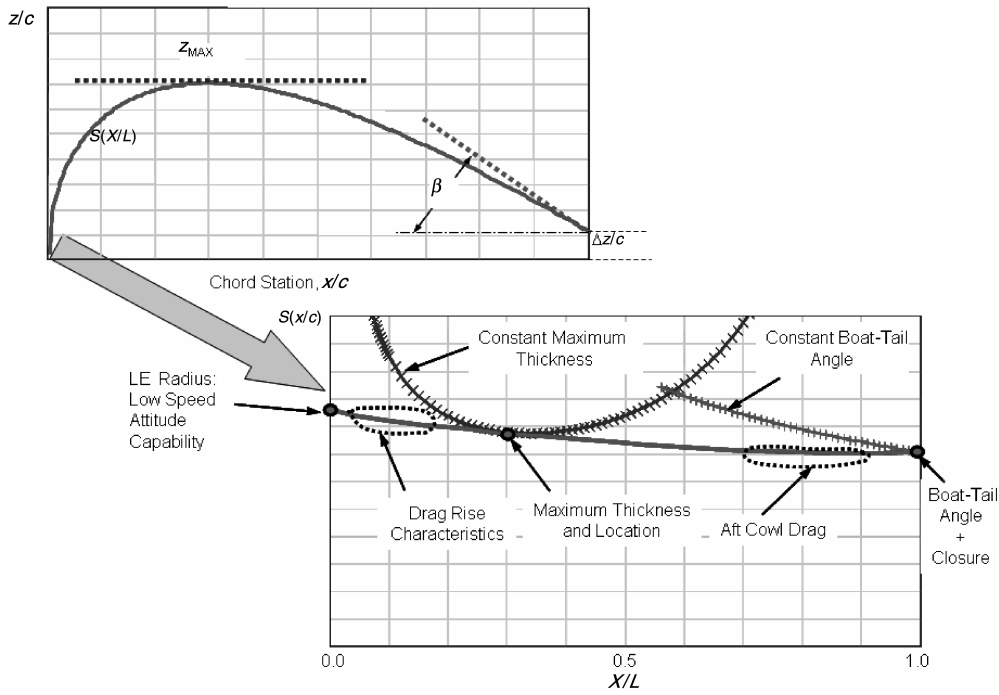
$$N1 = 0.75 \text{ and } N2 = 0.75$$

Fig. 1   Example of an airfoil geometric transformation.

define the radius distribution of a Sears–Haack body. The Sears–Haack body is the minimum drag supersonic body for a given volume.

$$N1 = 0.75 \text{ and } N2 = 0.25$$

define a low-drag projectile.

$$N1 = 1.0 \text{ and } N2 = 0.001$$

define a cone or wedge airfoil.

$$N1 = 0.001 \text{ and } N2 = 0.001$$

define a rectangle, circular duct, or a circular rod.

The class function is used to define general classes of geometries, whereas the shape function is used to define specific shapes within the geometry class.

Defining an airfoil shape function and specifying its geometry class is equivalent to defining the actual airfoil coordinates, which can be obtained from the shape function and class function as

$$\zeta(\psi) = C_{N2}^{N1}(\psi)S(\psi) + \psi\zeta_T \qquad (7)$$

IV.   Representing the Shape Function

A number of different techniques of representing the shape function for describing various geometries will be briefly described in this paper. The simplest approach is illustrated in Fig. 2. The figure shows the fundamental baseline airfoil geometry derived from the simplest of all shape functions, the unit shape function: $S(\psi) = 1$. Simple variations of the baseline airfoil are also shown with individual parametric changes of the leading-edge radius, and of the trailing-edge boat-tail angle.

The figure on the left shows changes in the leading-edge radius and the front portion of the airfoil obtained by varying the value of $S(0)$ with a quadratic equation that is tangent to the Z_{max} curve at x/c for Z_{max}. The maximum thickness, maximum thickness location, and boat-tail angle remained constant.

The figure on the right shows variations in boat-tail angle obtained by changing the value of the shape factor at the aft end, $x/c = 1$, whereas the front of the airfoil is unchanged. In each of these examples, the airfoil shape changes are controlled by a single variable and in all cases the resulting airfoil is both smooth and continuous.

Figure 3 shows a five-variable definition of a symmetric $C_{1.0}^{0.5}(\psi)$ airfoil shape function. The corresponding airfoil geometry is also shown. The variables include 1) maximum thickness,
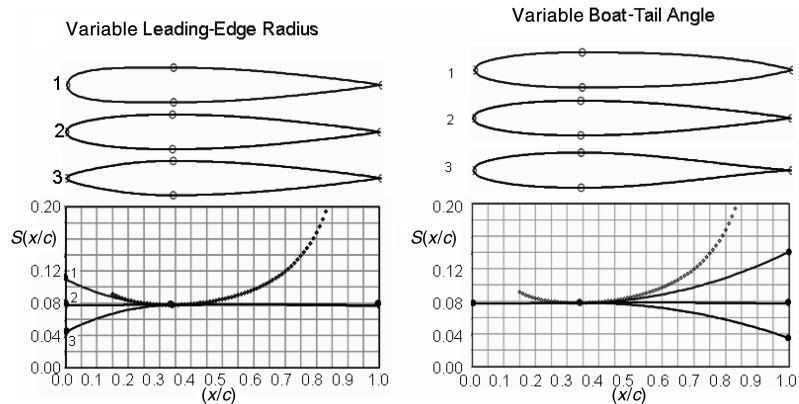

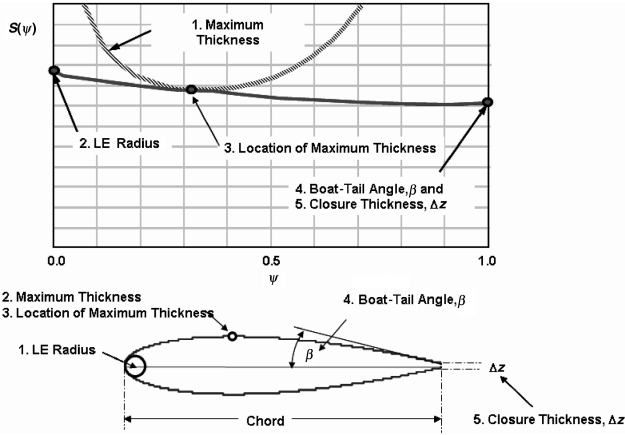Fig. 2   Examples of one variable airfoil variations.

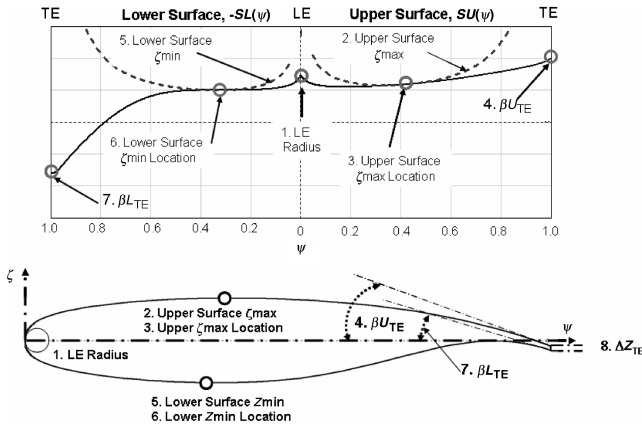Fig. 3 Symmetric airfoil five variables definition.

Fig. 4 Cambered airfoil seven variables definition.

2) leading-edge radius, 3) location of maximum thickness, 4) boat-tail angle, and 5) closure thickness.

A cambered airfoil can be defined by applying the same technique to both the upper and lower surfaces. In this instance, the magnitude of the value of the shape function at the nose $S(0)$ of the upper surface is equal to that on the lower surface. This ensures that the leading-edge radius is continuous from the upper to the lower surface of the airfoil. The value of the half-thickness at the trailing edge is also equal for both surfaces. Consequently, as shown in Fig. 4, seven variables would be required to define the aforementioned set of parameters for a cambered airfoil. Eight variables would be required for an airfoil with a nonzero trailing-edge thickness.

In the examples shown in Figs. 3 and 4, the key defining parameters for the airfoils are all easily controllable on the defining shape function.

V.   Airfoil Decomposition into Component Shapes

In Fig. 5, it is shown that the unit shape function defined by $S(\psi) = 1$, can be decomposed into two component shape functions.

$S1(\psi) = 1 - \psi$, which corresponds to an airfoil with a round nose and zero boat-tail angle

$S2(\psi) = \psi$, which corresponds to an airfoil with zero nose radius and a finite boat-tail angle.

An arbitrary scaling factor KR is shown in the figure as a weighting factor in the equations for the two component airfoils. By varying the scaling factor KR, the magnitudes of the leading-edge radius and the boat-tail angle can be changed. This results in a family of airfoils of varying leading-edge radius, boat-tail angle, and location of maximum thickness.

The unit shape function can be further decomposed into component airfoils by representing the shape function with a Bernstein polynomial. The Bernstein polynomial of any order n is composed of the $n + 1$ terms of the form

$$S_{r,n}(x) = K_{r,n}x^r(1-x)^{n-r} \tag{8}$$

where $r = 0–n$, and $n = $ order of the Bernstein polynomial.

In the preceding equation, the coefficients factors $K_{r,n}$ are binomial coefficients defined as

$$K_{r,n} \equiv \binom{n}{r} \equiv \frac{n!}{r!(n-r)!} \tag{9}$$

A series of Bernstein polynomials are shown in Fig. 6, in the form of Pascal's triangle.

The representation of the unit shape function in terms of increasing orders of the Bernstein polynomials provides a systematic decomposition of the unit shape function into scalable components. This is the direct result of the "partition of unity" property which states that the sum of the terms, which make up a Bernstein polynomial of any order, over the interval of 0–1, is equal to one. This means that every Bernstein polynomial represents the unit shape function. Consequently, the individual terms in the polynomial can be scaled to define an extensive variety of airfoil geometries.

For any order of Bernstein polynomial selected to represent the unit shape function, only the first term defines the leading-edge radius and only the last term defines the boat-tail angle. The other in-between terms are "shaping terms" that neither affect the leading-edge radius nor the trailing-edge boat-tail angle.

Examples of decompositions of the unit shape function using various orders of Bernstein polynomials are shown in Fig. 7 along with the corresponding component airfoils.

The locations of the peaks of the component S functions are equally spaced along the chord at stations which are defined by the equation

$$(\psi)_{S\max i} = \frac{i}{n} \quad \text{for } i = 0–n \tag{10}$$

The corresponding locations of the peaks of the component airfoils are also equally spaced along the chord of the airfoil and are defined in terms of the class function exponents and the order of the Bernstein
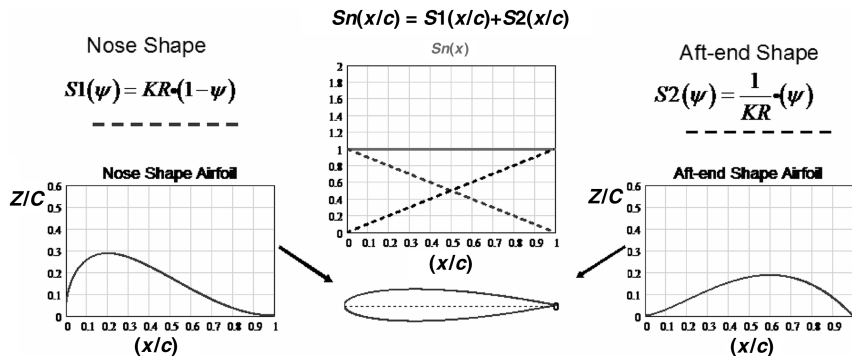

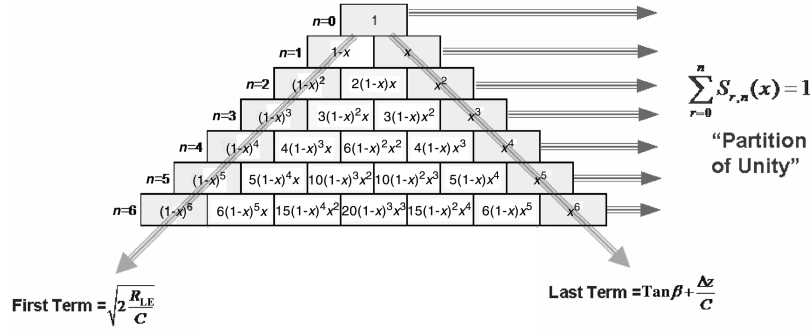Fig. 5 Airfoil decomposition into component shapes or basis functions.

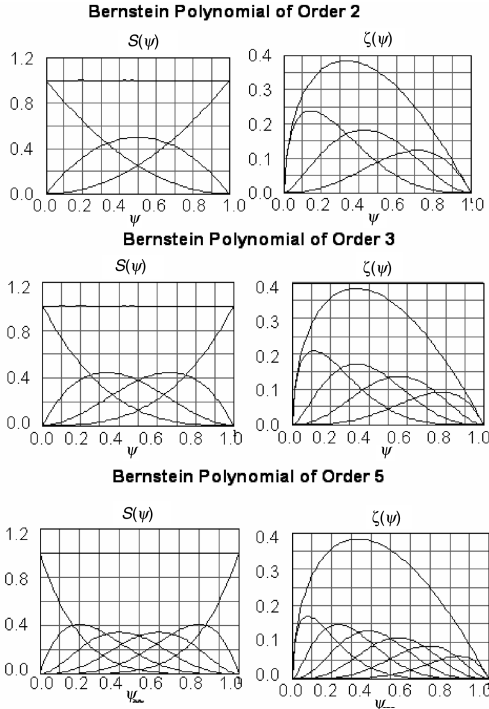Fig. 6 Bernstein polynomial decomposition of the unit shape function.

Fig. 7 Bernstein polynomial provides "natural shapes."

polynomial by the equation

$$(\psi)_{Z\max} = \frac{N1 + i}{N1 + N2 + n} \quad \text{for } i = 0\text{–}n \quad (11)$$

The technique of using Bernstein polynomials to represent the shape function of an airfoil in reality defines a set of component airfoil geometries that can be scaled and then summed to represent a variety of airfoil shapes.

VI. Airfoils Defined Using Bernstein Polynomials Representation of the Unit Shape Function

The upper and lower surfaces of a cambered airfoil can each be defined using Bernstein polynomials of any selected order n to describe a set of component shape functions that are scaled by "to be determined" coefficients as shown in the following equations.

The component shape functions are defined as

$$S_i(\psi) = K_i \psi^i (1 - \psi)^{n-i} \quad (12)$$

where the term K_i is the binomial coefficient, which is defined as

$$K_i \equiv \binom{n}{i} = \frac{n!}{i!(n-i)!} \quad (13)$$

Let the trailing-edge thickness ratios for the upper and lower surface of an airfoil be defined as

$$\Delta\xi_U = \frac{zu_{\text{TE}}}{C} \quad \text{and} \quad \Delta\xi_L = \frac{zl_{\text{TE}}}{C} \quad (14)$$

The class function for the airfoil is

$$C_{N2}^{N1}(\psi) = \psi^{N1}(1 - \psi)^{N2} \quad (15)$$

The overall shape function equation for the upper surface is

$$Su(\psi) = \sum_{i=1}^{n} Au_i S_i(\psi) \quad (16)$$

The upper surface defining equation is

$$(\zeta)_{\text{upper}} = C_{N2}^{N1}(\psi)Sl(\psi) + \psi\Delta\xi_{\text{upper}} \quad (17)$$

The lower surface is similarly defined by the equations

$$Sl(\psi) = \sum_{i=1}^{n} Al_i S_i(\psi) \quad (18)$$

and

$$(\zeta)_{\text{lower}} = C_{N2}^{N1}(\psi)Sl(\psi) + \psi\Delta\xi_{\text{lower}} \quad (19)$$

The coefficients Au_i and Al_i can be determined by a variety of techniques depending on the objective of the particular study. Some examples include 1) variables in a numerical design optimization application, 2) least-squares fit to match a specified geometry, and 3) parametric shape variations.

The method of using Bernstein polynomials to represent an airfoil has the following unique and very powerful properties [9]:

1) This airfoil representation technique captures the entire design space of smooth airfoils.

2) Every airfoil in the entire design space can be derived from the unit shape function airfoil.

3) Every airfoil in the design space is therefore derivable from every other airfoil.

A key convergence question relative to the class function/shape function geometry method for defining airfoils, nacelles, or bodies of revolution is the following: What orders of Bernstein polynomials (BPO) are required to capture enough of a meaningful design space to contain a true optimum design?

A two-step approach was defined to obtain the answer for this question:

1) Actual airfoil geometry and approximated airfoil geometries were compared for a wide variety of airfoils.

a) Various orders of Bernstein polynomials were used to approximate the shape functions computed from the defined airfoil coordinates. The coefficients for the component Bernstein polynomial shape functions were determined by least-squares fits to match the selected airfoil upper and lower surface shape functions.

b) Statistical measures, such as residual differences, standard deviations, and correlation functions, were computed to quantify the "mathematical goodness" of the representations for each of the study airfoils.

c) Detailed comparisons were made of the surface slopes, second derivatives, and curvature for the actual and the approximate airfoil shapes.

d) A wide variety of optimum and nonoptimum, symmetric, and cambered airfoil geometries were analyzed in this manner.

2) The actual airfoils and the corresponding approximate airfoils using computational fluid dynamics (CFD) analyses were made using TRANAIR full-potential code [11,12] with coupled boundary layer.

More than 30 airfoils have been analyzed using this process. These include symmetric NACA airfoils, cambered NACA airfoils, high-lift airfoils, natural laminar flow airfoils, shock-free airfoils, supercritical airfoils, and transonic multipoint optimized airfoils. Results of the analyses of some of these airfoils were shown and discussed in [9]. An example of this evaluation process is shown next to demonstrate the rate of convergence of a Bernstein polynomial shape function airfoil representation to the corresponding specified airfoil geometry with increasing orders of the Bernstein polynomial.

VII. Example Airfoil Representation: RAE2822

Examples of the type of in-depth convergence studies that were conducted to determine the ability of the class function/shape function methodology to represent a wide variety of airfoils are shown for a typical supercritical airfoil, RAE2822, in Figs. 8–11.

The airfoil geometry as "officially" defined by 130 x, z coordinates is shown in Fig. 8. The shape functions for the upper and lower surface, as calculated from these coordinates, are also shown. The shape function curves are seen to be very simple curves as compared with the actual airfoil upper and lower surfaces.

Shape functions calculated by the method of least squares to match the defined airfoil shape functions corresponding to increasing orders of Bernstein's polynomials are compared with the shape function determined from the actual RAE2822 geometry coordinates in Fig. 9. The corresponding approximate airfoil geometries are shown in Fig. 10. The locations of the peaks of the component shape functions
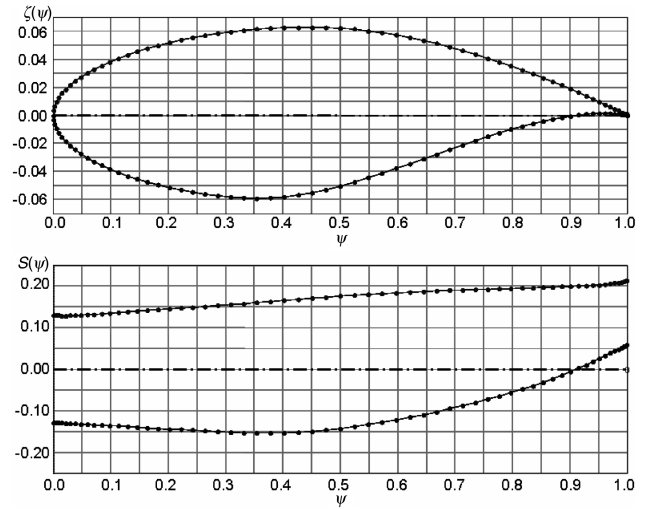

Fig. 8   RAE2822 airfoil geometry (defined by 130 X, Z coordinates).

and the corresponding component airfoils are indicated in the individual figures.

The residual differences between the defined airfoil and approximated airfoil shape functions, and the surface coordinates, are also shown in the figures. The differences between the actual and the approximated shape functions and surface coordinates are hardly discernible even for the Bernstein polynomial of order three (BPO3) representation. The oscillating nature of the residual curves is typical of any least-squares fit.

The results obtained with BPO5 and BPO8 show that the residual differences rapidly and uniformly vanish with increasing order of the representing Bernstein polynomial. The differences between the BPO5 and BPO8 approximate airfoils and the actual geometry are well within the indicated typical wind-tunnel model tolerances.

Two statistical measures of the quality of the shape function representative of the RAE2822 airfoil geometry are shown in Fig. 11 as a function of the order of the Bernstein polynomial. These include 1σ standard deviation of the residuals for both the shape function and airfoil coordinates, and the correlation coefficient r^2, which is
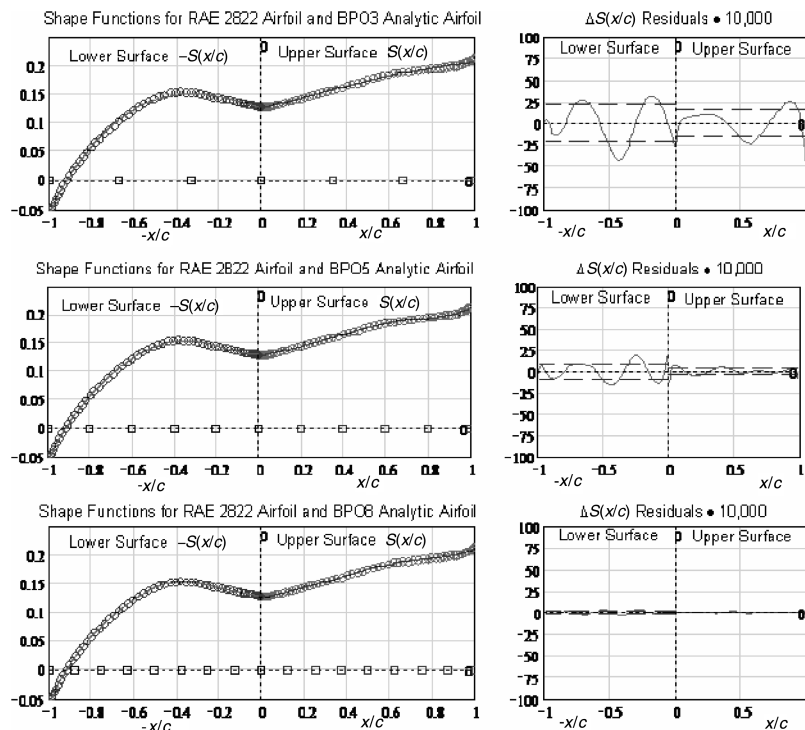

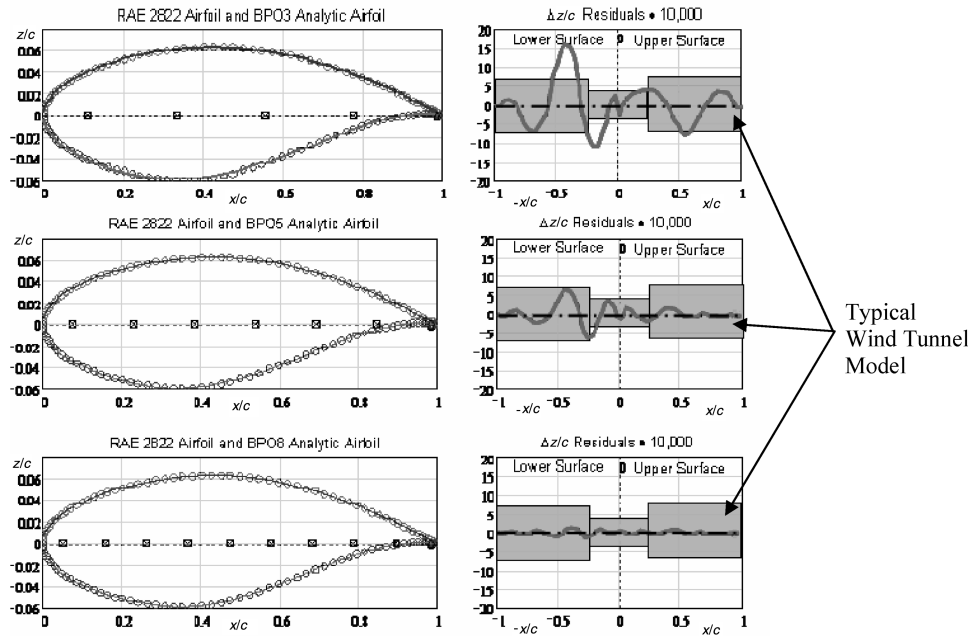Fig. 9   RAE2822 shape function convergence study.

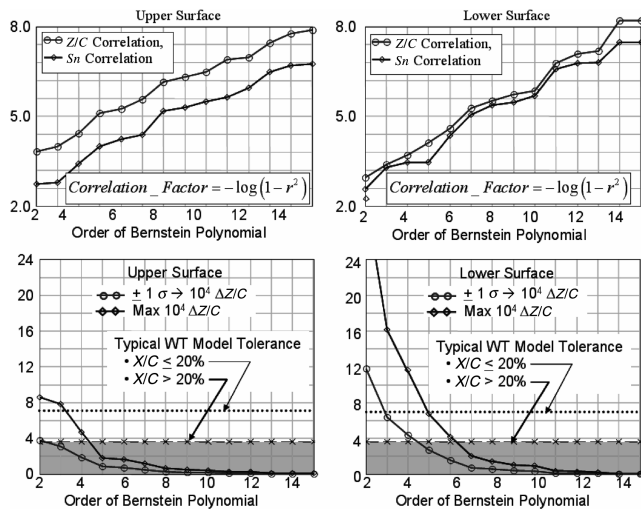Fig. 10   RAE2822 airfoil shape convergence study.

Fig. 11   RAE2822 airfoil statistical convergence.

expressed here in terms of a correlation factor, defined as

$$\text{correlation factor} = -\log(1 - r^2) \qquad (20)$$

The correlation factor equals the number of initial nines in the correlation coefficients between the airfoil data and the corresponding approximated data. For example, a correlation factor of 5.0 means that $r^2 = 0.99999$.

The results of the statistical analyses of the quality of the agreement between the approximating airfoils and the numerical definitions show that for a BPO of about six and greater that the analytically defined airfoils essentially become statistically identical with the actual airfoil definition.

The slopes and second derivatives obtained with various orders of BP shape functions are compared with slopes and second derivatives obtained from the RAE2822 airfoil coordinates in Fig. 12. The airfoil slopes and second derivatives both numerically go to infinity near the nose of the airfoil and, therefore, it is difficult to see differences between matched geometry and actual airfoil geometry in the nose region. The singularity in the first derivative can be eliminated through the use of a transformed slope obtained by multiplying the slope by $(x/c)^{0.5}$. Similarly, the singularity in the second

derivative can be removed by multiplying the second derivatives by $(x/c)^{1.5}$.

Negative values of the slopes and second derivatives are shown for the lower surface to provide a clearer illustration of the differences of the upper and lower surface geometry characteristics.

The transformed values of the slopes and of the second derivatives allow the differences between values determined for the analytically defined airfoils and those determined from the official numerical definition of the RAE2822 to be easily seen. The analytical slopes and second derivatives of the approximate airfoils rapidly converge to match the corresponding values determined from the actual airfoil definition.

Although not shown in the figure, as the BPO continues to increase, the differences in even the finest details between the airfoil characteristics determined from the analytical representations and the actual airfoil geometry continued to vanish.

Calculations of surface pressure distributions CP between the actual and represented geometries were made using the TRANAIR [11,12] full-potential CFD code with coupled boundary layer for a series of shape function derived analytical airfoils with BPO2–BPO15 shape function definitions.

In all cases, the defining inputs stations for the TRANAIR analyses were identical to the official defining stations for the RAE2822. Some of the results from these RAE2822 analyses are shown in Fig. 13 for a series of analytical representations corresponding to PBO2, BPO4, BPO6, and BPO8 shape function defined airfoils.

The pressure distribution for even the BPO2 representation, which is defined by only six variables for representing both the upper and lower surfaces of the airfoil, appear to be surprisingly close to the actual airfoil upper surface pressure distribution. The predictions of the BPO6 and BPO8 analytic airfoils closely match the upper surface pressure distributions for the numerically defined airfoil.

The two lowest order BP airfoils have very slight differences in the lower surface CPs from those of the numerically defined airfoil. The upper and lower CP distributions for all the BPO6 and above airfoils appeared to exactly match those for the RAE2822 numerical definition.

Comparisons of the lift and drag predictions for the approximating airfoils and the numerically defined airfoil are shown in Fig. 14.

The lift predictions for all BPO5 and greater airfoils matched the RAE2822 predictions. The drag predictions for BPO8 and above agree exactly with the predictions for the actual RAE2822. Both the
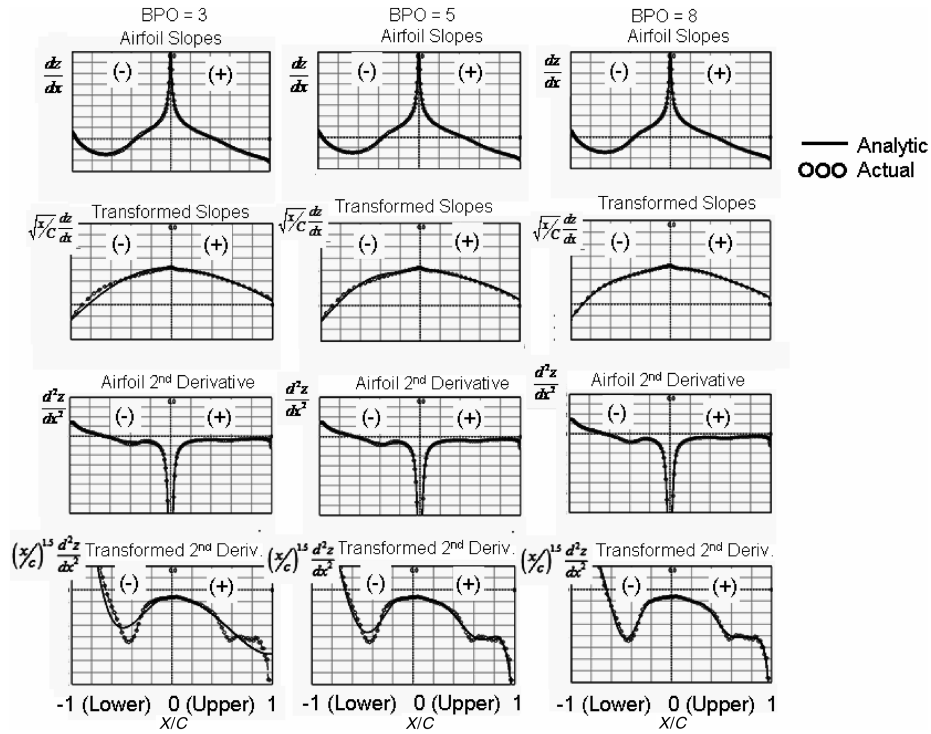
Fig. 12   RAE2822 airfoil slope and second derivatives convergence.
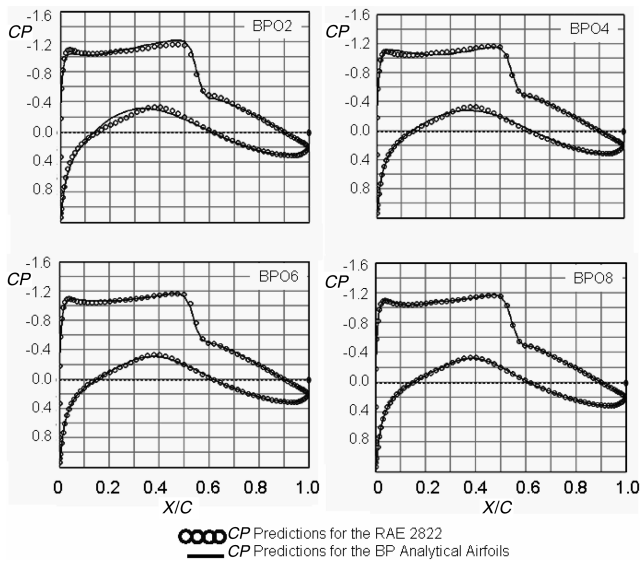

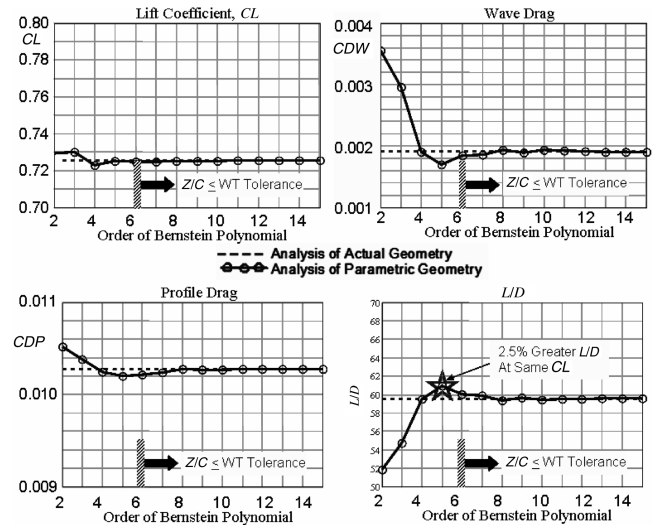**Fig. 13   RAE2822 pressure distribution convergence.**

Fig. 14   RAE2822 aerodynamic force convergence.

profile drag and wave drag for the BPO5 airfoil are less than that of the baseline RAE2822 airfoil, even though the lift predictions are identical. Consequently, the least-squares shape function matching study which was certainly not intended as a design optimization study, did result in an airfoil geometry with a 2.5% increase in lift/ drag ratio over that of the RAE2822 airfoil. This is most likely the result of the smoothing capability inherent in the class function/shape function methodology.

The lift predictions for all BPO5 and greater airfoils matched the RAE2822 predictions. The drag predictions and pressure distributions for BPO8 and above agreed exactly with the RAE2822 predictions.

The results of the lift, drag, and pitching moment predictions for both zero angle of attack and an angle of attack of 2.31 deg are shown in Fig. 15 for the BPO8 airfoil and the actual RAE2822 airfoil definition. The force predictions for the BPO8 airfoil exactly match those of the RAE2822.

Similar results were also shown in [9] for a number of other airfoil geometries. The results of the geometry, CP, and force comparisons implied that a relatively low-order BP shape function airfoil with only a relatively small number of variables can closely represent any airfoil.

The mathematical simplicity of the shape function representation of an airfoil is clearly evident for the example of the RAE2822 airfoil in Fig. 16. In this figure, the surfaces slopes, second derivatives, and surface curvature for the airfoil surfaces are compared with the corresponding values for the upper and lower surface shape function.

The slopes and second derivatives of the RAE2822 airfoil are infinite at the nose, and the curvature varies greatly over the surface of the airfoil. The slopes and second derivatives are finite, and everywhere small for the RAE2822 shape function, and the curvature of the shape function is essentially zero. This clearly shows the distinct advantage of mathematical simplicity that the shape function airfoil representation methodology has relative to the use of the actual coordinates of the airfoil.
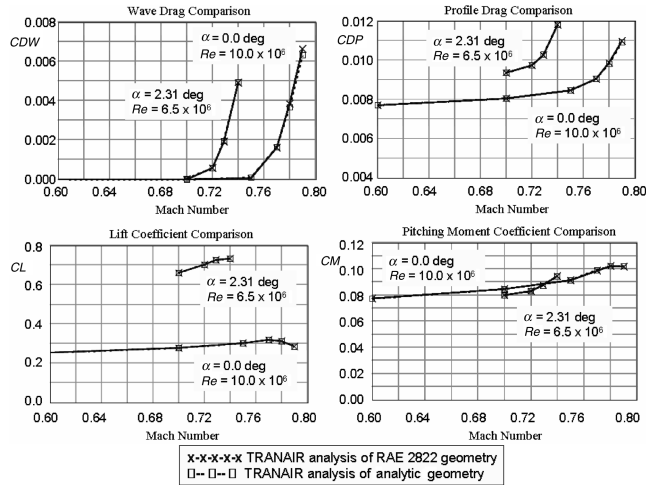
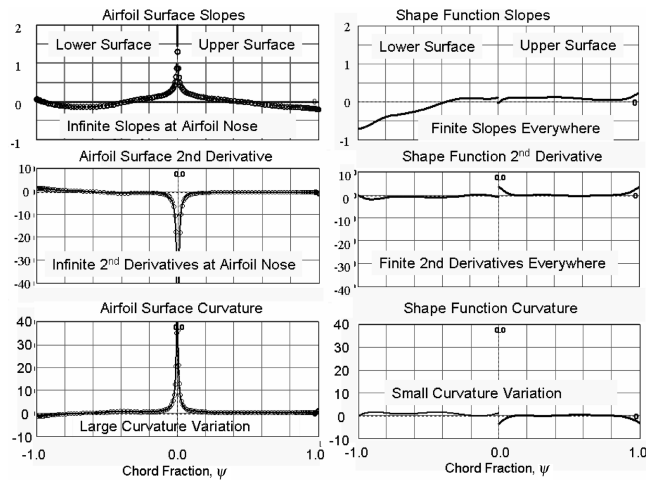**Fig. 15   RAE2822 aerodynamic force comparisons BPO8.**

Fig. 16   Mathematical simplicity of the shape function: RAE2822.

The results of the previously reported extensive investigations [9] of the adequacy of the shape function methodology using Bernstein polynomials to represent a wide variety of airfoils showed that a relatively low-order Bernstein polynomial (typically BPO6 to BPO9) matched the airfoils geometries, slopes, and second derivatives, as well as the pressure distributions and aerodynamic forces [9]. The results also indicated that lower-order Bernstein polynomials, corresponding to fewer design variables (perhaps BPO4 to BPO6), should be adequate for developing optimum designs.

The methodology offers the option for a systematic approach for design optimization. The optimization process can initially be conducted with a family of component airfoil shapes corresponding to a low-order BP representation for the shape function to obtain an optimum design. The order of the BP can then be increased to conduct another optimization to determine if a better optimum design is achieved. Increasing the order of the BP is a systematic way to increase the number of design variables, which corresponds to extending the design space, and thereby exploring the convergence of an optimum solution.

In the previously discussed studies, the BP shape function airfoil definitions used the same order BP for both the upper and lower surfaces. Although this is not a requirement, it does provide a very convenient means for determining the component camber and thickness distributions for an airfoil by simply adding and subtracting the unit shape function scaling coefficients as shown in Fig. 17.

The discussions so far have been focused on two-dimensional round-nose/sharp aft-end airfoils. However, the class function/shape function methodology can also be used equally well for defining the radius distribution of axisymmetric geometries.

VIII.   Extension to Body Cross Section Geometries

The shape function/class function methodology of representing a two-dimensional or axisymmetric geometry will now be shown to be directly applicable for representation of the cross-sectional shapes of the class 2 geometry components which are the "body type" geometries.
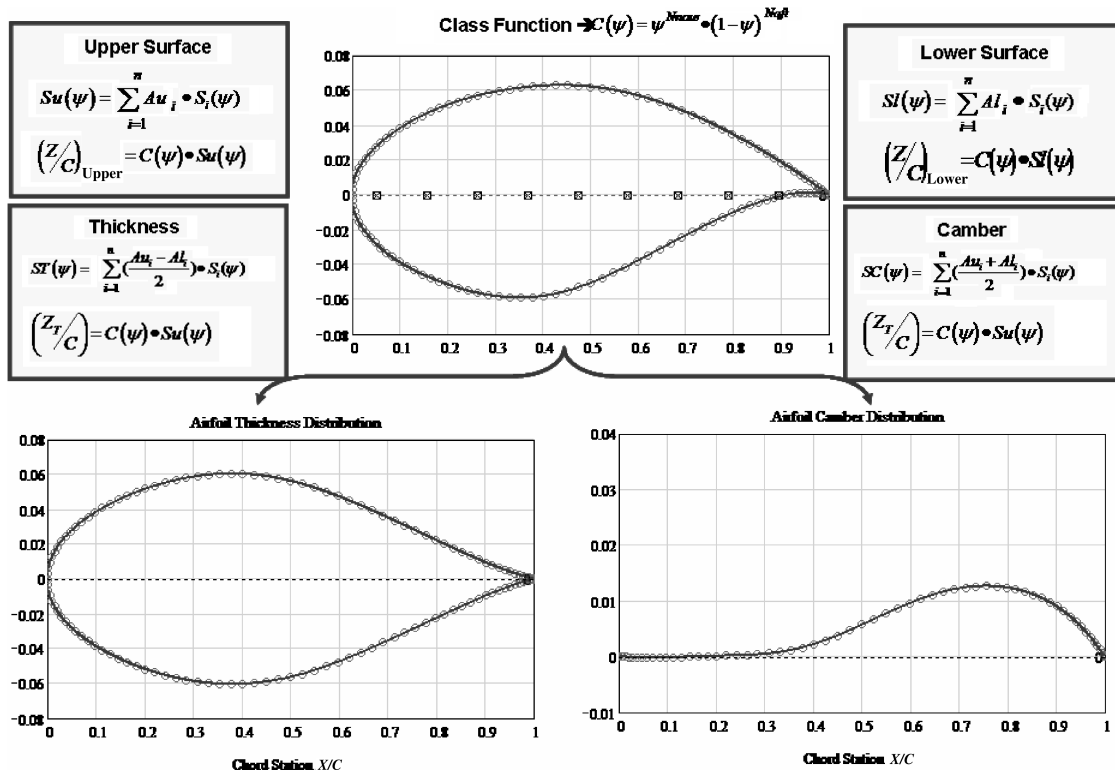

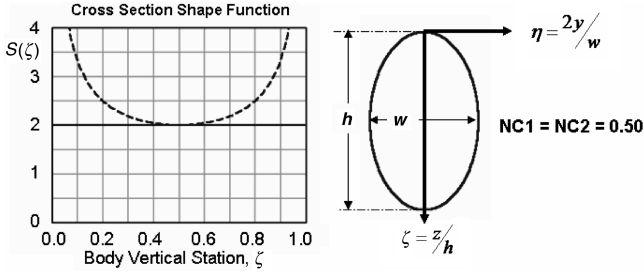**Fig. 17   Simple decomposition of an airfoil into thickness and camber.**

Fig. 18   Shape function/class function representation of a body cross section.

Let us initially assume that a body cross section is laterally symmetric and has the shape of an ellipse as shown in Fig. 18. We will then subsequently generalize the results using the class function to other cross-sectional geometries.

The equation for an ellipse in the coordinate system shown in the figure is

$$\left(\frac{2Y}{w}\right)^2 + \left(\frac{2Z-h}{h}\right)^2 = 1 \tag{21}$$

Let $\eta = 2y/w$ and $\zeta = z/h$.

The ellipse equation becomes $\eta^2 + (2\zeta - 1)^2 = 1$ or $\eta = 2\sqrt{\zeta} \cdot \sqrt{1-\zeta}$.

The cross section can then be expressed in terms the class function and shape function as

$$\eta = S(\zeta)C_{0.5}^{0.5}(\zeta) \tag{22}$$

The cross section shape function is simply a constant: $S(\eta) = 2$. The opposite side is defined by the condition of lateral symmetry. As shown in Fig. 19, varying the exponents of the class function can provide a wide variety of body cross section shapes.

This lateral representation of a cross section is very convenient for use in defining geometries such as lifting bodies. Another approach to represent a cross section, that is perhaps more useful for defining nacelle and fuselage cross sections, is to use a class function to describe the upper lobe and another class function to describe the lower lobe of a body cross section, each as shown in Fig. 20. This is very similar to the process for defining a cambered airfoil. Let us assume initially that a body cross section is laterally symmetric and has the shape of an ellipse. We will then subsequently generalize the results using other values for the class functions.
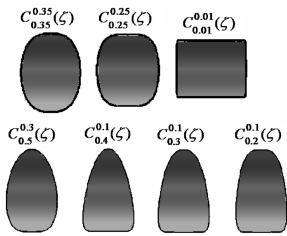

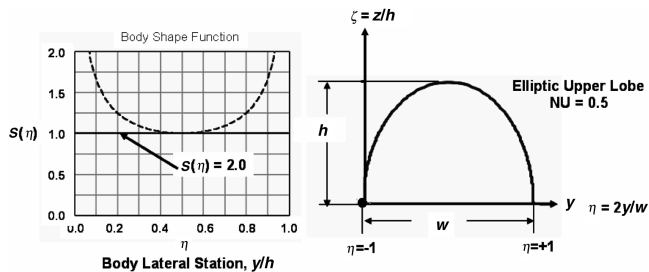**Fig. 19   Various body cross-sectional shapes.**

Fig. 20   Representation of a body upper or lower lobe shape.

The equation for the ellipse with the axes of the ellipse at the left edge can be expressed as

$$\zeta(\eta) = 2\eta^{0.5}(1-\eta)^{0.5} \tag{23}$$

where $\eta = y/w$ and $\zeta = z/h$.

The shape function for this upper lobe elliptic geometry is therefore

$$Su(\eta) = \frac{\zeta u(\eta)}{\eta^{\text{NC1}}(1-\eta)^{\text{NC2}}} = 2 \tag{24}$$

In the preceding equation, we have generalized the definition of the class function by using the variable exponents NC1 and NC2

$$C(\eta) = \eta^{\text{NC1}}(1-\eta)^{\text{NC2}} \tag{25}$$

The cross section geometry equation expressed in terms of the shape function and the class function becomes

$$\zeta u(\eta) = Su(\eta)C(\eta) \tag{26}$$

For an elliptic upper lobe shape, the shape function is a constant and equal to 2.0, and the class function exponents are NC1 = NC2 = 0.5.

In this case, the upper lobe defining equation is

$$\zeta u(\eta) = [Su(\eta) \equiv 2]Cu_{0.5}^{0.5}(\eta) \tag{27}$$

Figure 21 shows examples of a variety of cross section shapes that can be obtained by independently varying the class function coefficients for the upper and lower lobes of the body cross section.

The example cross sections shown in Figs. 19 and 21 were all obtained using simple unit shape functions with different class functions. Very general cross-sectional shapes can be generated by varying the shape function formulations in addition to the class functions. As shown in Fig. 22, changing the shape function for the upper body lobe can create upper surface bumps or fairings. In the
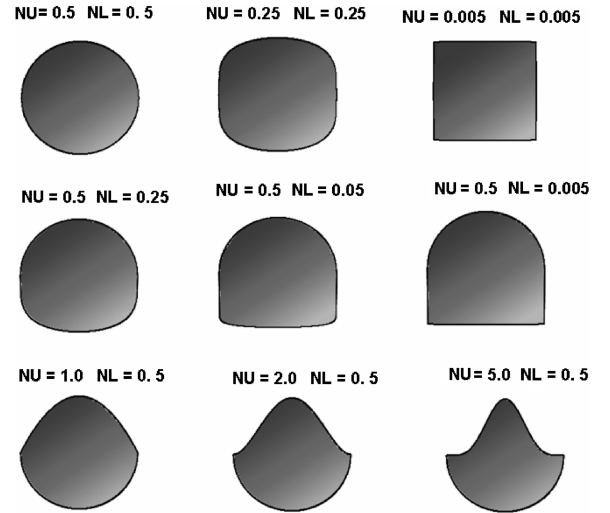

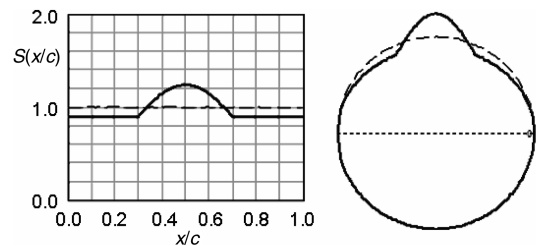**Fig. 21   Example upper lobe/lower lobe body cross sections.**

Fig. 22   Fuselage "bump" representation.

example shown, the geometry is representative of a cross section of a fuselage through the cockpit area.

IX. Extension to Arbitrary Three-Dimensional Geometries

Three-dimensional bodies in general can be represented as a distribution of the cross-sectional shapes.

The shape function/class function methodology can be used to describe both the fundamental cross-sectional shapes and the distribution of the shapes along the body axis, as shown for the simple case of a cube in Fig. 23.

The cross section shape function Sc and class function Cc are defined by the equations

$$Sc = 0.5^{2 \cdot NC} \tag{28}$$

$$Cc(\eta) = \eta^{NC}(1 - \eta)^{NC} \qquad \eta \to 0\text{–}1 \tag{29}$$

The distribution shape function Sd and class function Cd are defined by similar equations:

$$Sd = 0.5^{2 \cdot ND} \tag{30}$$

$$Cd(\psi) = \psi^{ND}(1 - \psi)^{ND} \qquad \psi \to 0\text{–}1 \tag{31}$$

NC and ND are the class function exponents.

As shown in Fig. 23, $L =$ the body length, $W =$ the body width, and $H =$ the body height.

The defining x, y, and z coordinates are given by the equations

$$x(\psi) = \psi \cdot L \tag{32}$$

$$y(\psi, \eta) = -[Sd \cdot Cd(\psi)] \cdot [1 - 2 \cdot \eta] \cdot \frac{W}{2} \tag{33}$$

$$z(\psi, \eta) = \pm[Sd \cdot Cd(\psi)] \cdot [Sc \cdot Cc(\eta)] \cdot \frac{H}{2} \tag{34}$$

For a simple unit cube, $L = W = H = 1$ and $NC = ND \simeq 0.001$.

Examples of various geometries determined using Eqs. (28–34), with various combinations of the class functions exponents, are shown in Fig. 24.

The third image in the figure is a solid circular cylinder having a distribution class function with exponents slightly above zero ($ND = 0.005$). As shown in the fourth image, when the distribution class function exponent is exactly zero ($ND = 0.0$), the geometry is a circular flow-through duct. A value of $ND = 0$ results in an open flow-through object, and a value of $ND \simeq 0.005$ results in a similar but solid geometry.
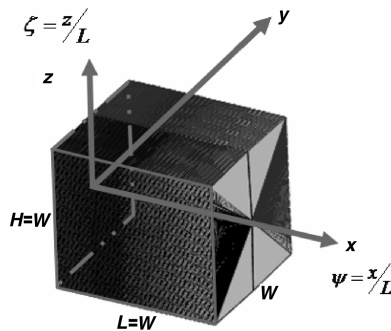

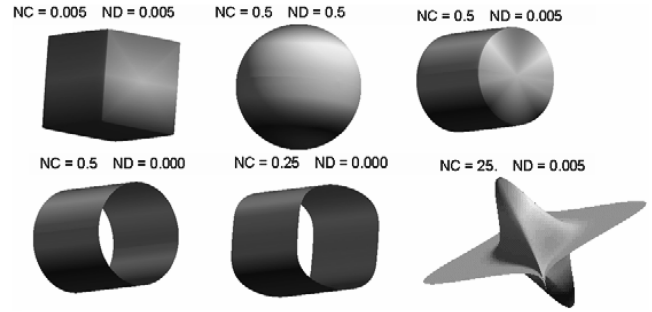**Fig. 23   Definitions of cross section shape and distribution.**

Fig. 24   Geometries derived as class function distribution of class function cross section shapes.
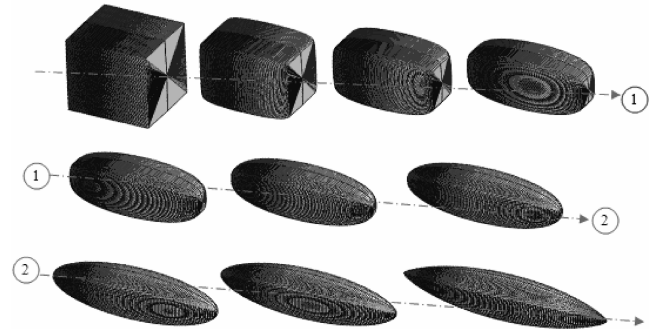

Fig. 25   Three variable transformation of a cube into a Sears–Haack body.

Figure 25 shows an example of using the shape function/class function methodology to make apparently significant geometry changes with very few design variables, by transforming a cube into an equal volume Sears–Haack body.

The circular cross section of the Sears–Haack body has unit shape function and class functions exponents equal to $Cs_{0.5}^{0.5}(\eta)$. The longitudinal radius distribution of a Sears–Haack body has a unit shape function and a class function equal to $Cd_{0.75}^{0.75}(\psi)$.

Consequently, the transformation of the cube into a Sears–Haack body is easily obtained by simultaneously increasing the cross section class function exponents from 0.005 to 0.5, and then increasing the longitudinal radius distribution class function exponents from 0.005 to 0.75, and increasing the length to keep the volume constant.

Figure 25 shows a number of intermediate geometries as the cube is smoothly transformed into the Sears–Haack body.

An example of transforming a constant area circular duct into a circular duct with geometry that varies from a circular inlet to a square-shaped nozzle, while maintaining a constant cross section area, can be easily defined using variable class function exponents as shown in Fig. 26.

The initial geometry shape at the inlet is a circular duct defined with a cross section class function with exponents equal to 0.5. The duct geometry, in this example, retains a constant cross section from 0 to 20% of the length. The last 5% length of the duct has a square cross section which has class function exponents equal to 0.001. The width/depth of the square were sized to match the circular inlet area.

In between 20 and 95% of the length, the class function exponents were decreased from 0.5 at 20% to 0.001 at 95% by a cubic variation with zero slopes at both ends. Along the transition region, the width and depth were scaled proportionally to keep the cross section area constant. The entire geometry is in reality driven by a single variable, the aft-end constant class function exponent.

This is an example of a "scalar" or "analytic" loft in which the geometry is generated by the analytic variation of the cross section class functions exponents along the length of the duct.
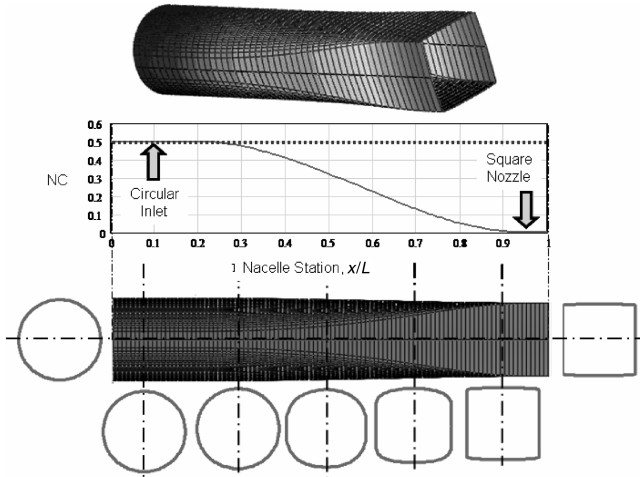
Fig. 26   One variable definition of a circular duct with a square nozzle.
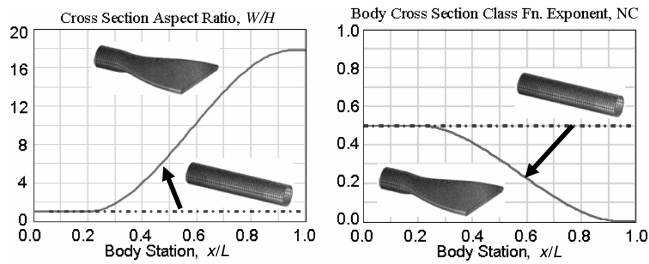

Fig. 27   Transformation of a circular duct to a thin rectangular nozzle (2 variables).

The transformation of a circular duct into a thin, wide, rectangular duct is shown in Fig. 27. This transformation was derived from the previous example by the addition of a single additional variable, the nozzle aspect ratio. This is the ratio of the exit nozzle width to the nozzle height. In this example, this additional variable varies from 1 to 17.8, as the cross section class function exponent varies from 0.5 to 0.005.

In Fig. 28, using a technique similar to that used to define the geometries in Figs. 26 and 27, a circular duct is transformed into a geometric shape that appears very similar to a supersonic aircraft configuration. This geometric transformation was obtained with a total of four design variables. The four design variables included 1) longitudinal class function exponents ND1, ND2; 2) aft-end cross section class function exponent NC (figure A); and 3) the width to height ratio at the aft end W/H (figure B).

Figure 28 also shows a series of cross section cuts through the final configuration to illustrate the smoothness of the geometry transition.

X.   Detailed Nacelle Design: Two Options

Let us now use the class function/shape function transformation to develop the detailed definition of a nacelle with just a few design parameters. There are two options for using class functions and shape functions for defining a nacelle. These include the following:

1) Define longitudinal profile shapes for crown line, maximum half-breadth, and keel line, and then distribe these profiles circumferentially around the longitudinal axis to define the nacelle geometry.

2) Define cross section shapes and distribute the shapes along the longitudinal axis.

In the discussions that follow, we will focus on the first option, because this will provide a demonstration of a combination of many of the concepts that have been shown in this paper and in the previous studies [9]. The objective is to develop a detailed nacelle definition with the use of very few design variables.
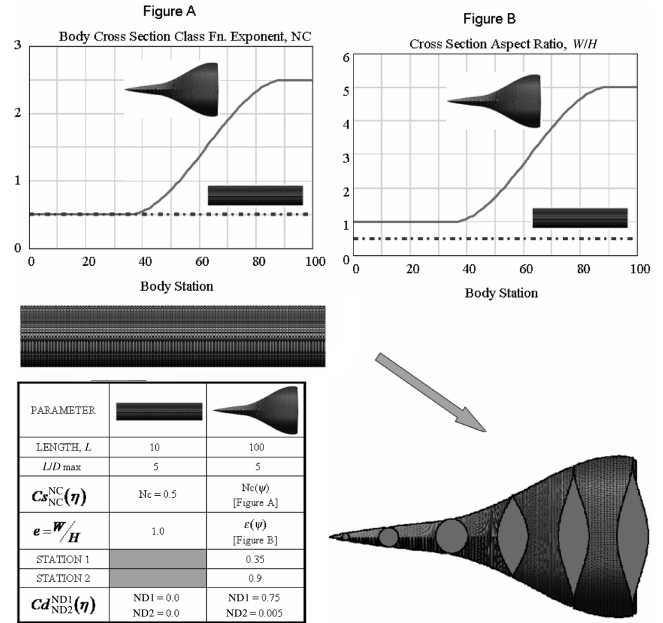

Fig. 28   Transformation of a circular cylinder in a supersonic transport.

Figure 29 shows a common approach that is often used to define a nacelle using airfoil-type sections for the crown line, keel line, and maximum half-breadth shapes. In this example, the basic airfoil geometries are represented by a BP5 shape function definition for a supercritical type airfoil, which therefore has six defining variables.

The keel line airfoil and the maximum half-breadth airfoils in this example are both parametrically modified forward of the maximum thickness station to increase the leading-edge radius in the former case and decrease the leading edge in the latter case. This results in the addition of two more defining variables corresponding to the desired leading-edge radii.

The external cross-sectional shape of the nacelle between the crown, maximum half-breadth, and keel is defined by an upper lobe class function with the exponent NU. The lower lobe of the nacelle between the maximum half-breadth and the keel line is similarly defined by lower lobe class function with the exponent NL. The distribution of cross-sectional shapes along the centerline of the nacelle is then defined by the variation of the class function exponents along the length of the nacelle, as shown in Fig. 30.

The upper lobe for the entire nacelle is defined using a constant class function exponent of 0.5. This results in an elliptic/circular cross-sectional shape distribution between the crown line and the maximum half-breadth defining geometries.

The lower lobe cross section class function exponents equal 0.25 out to defining station 1 which is located at 40% of the nacelle length. This results in a "squashed" shape distribution from the maximum half-breadth airfoil to the keel line airfoil over the front portion of the nacelle. The lower lobe aft of defining station 2, which occurs at 80% of the nacelle length, is circular with a class function exponent equal to 0.5. Consequently, this results in an axisymmetric nozzle geometry. In between station 1 and station 2, the lower lobe shape joining the maximum half-breadth geometry and the keel geometry varies smoothly from a squashed section at station 1 to a circular section at station 2. The cross-sectional shape distribution is therefore defined entirely by the following four design variables: 1) upper lobe class function exponents NU; 2) lower lobe class functions NL; 3) end of squashed lower lobe station, station 1; 4) start of circular lower lobe station, station 2.

The inlet definition is shown in Fig. 31. The internal inlet cross section shape and leading-edge radii distribution were defined to match the external cowl cross section shape and streamwise leading-edge radius distribution at the nose of the nacelle. The internal inlet shape then varied smoothly from the squashed shape at inlet lip to a circular cross section at the throat station. The internal shape was
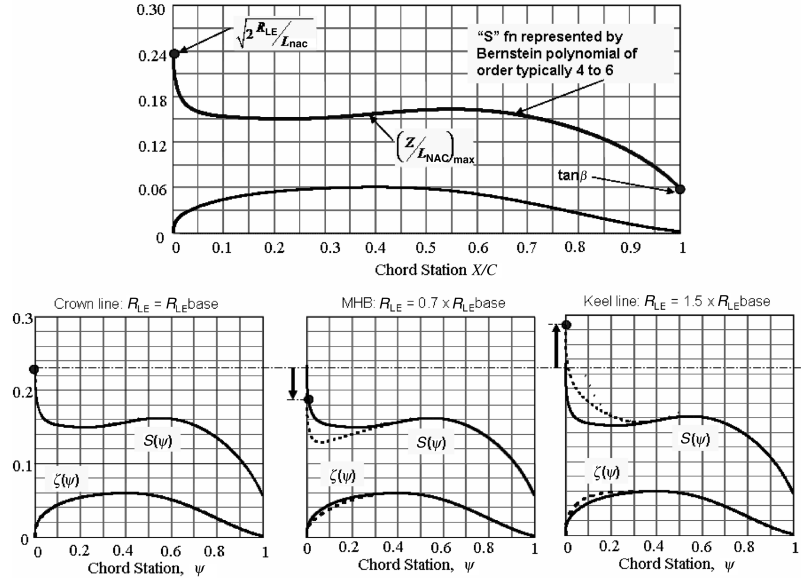
Fig. 29 Nacelle crown line, keel line, and maximum half-breadth definitions (8 variables).
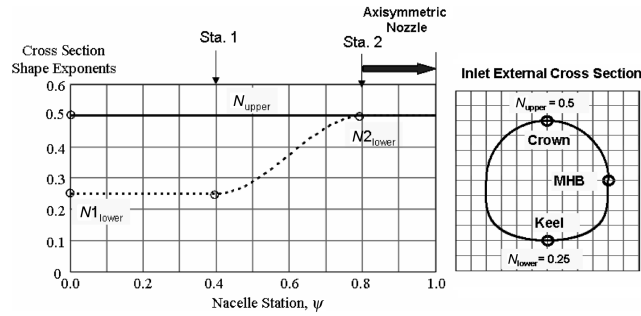

Fig. 30 Nacelle shape distribution radially around the nacelle centerline (4 variables).
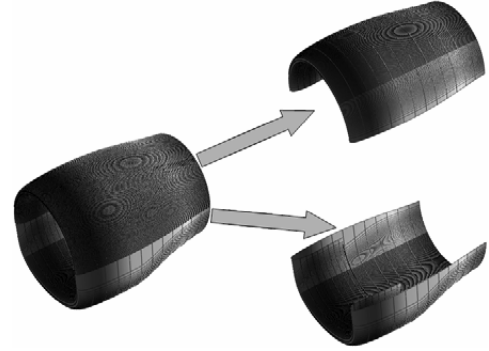

Fig. 31 Nacelle inlet geometry definition (4 variables).

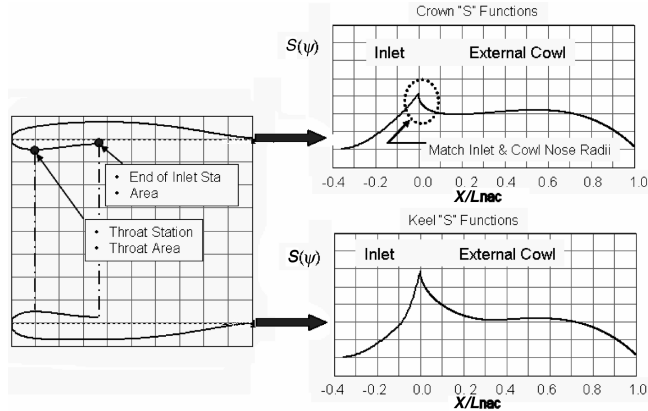Fig. 32 Total nacelle external shape and inlet geometry definition (15 variables).

defined as circular aft of the throat station to the end of the inlet length.

The entire internal inlet geometry required only four more defining variables. These include 1) throat station, 2) throat area, 3) end of inlet station, and 4) end of inlet area.

The complete nacelle geometry as defined by the aforementioned 15 total nacelle design variables is shown in Fig. 32. The geometry is seen to be smooth and continuous everywhere.

Based on this example, it would appear that for aerodynamic design optimization of the external shape of a nacelle, relatively few variables would be required to capture a very large design space of realistic smooth continuous geometries.

XI. Three-Dimensional Wing Definition Using the Class Function/Shape Function Transformation Method

A three-dimensional wing can be considered as a distribution of airfoils across the wing span. Consequently, we can use the previously discussed class functions and shape functions to obtain analytical definitions of the wing airfoil sections and then simply distribute the analytical formulations across the wing span to completely define a wing. In this section, we will first develop the analytical definition for any arbitrary wing. We will illustrate the use the methodology initially with a number of simple applications. This will be followed by an examination of application of the methodology to detailed subsonic and supersonic wings definitions.

A typical wing airfoil section is shown in Fig. 33. The analytical definition of a local wing airfoil section is similar to the airfoil definition [Eq. (1)] with two additional parameters that include the local wing shear and the local wing twist angle.

$$\zeta_U(\psi, \eta) = \zeta_N(\eta) + C_{1.0}^{0.5}(\psi)S_U(\psi, \eta) + \psi[\zeta_T(\eta) - \tan \alpha_T(\eta)]$$

(35)

where
fraction of local chord

$$\psi = \frac{x - x_{LE}(\eta)}{c(\eta)}$$

nondimensional semispan station $\eta = 2y/b$
local leading-edge coordinate $x_{LE}(\eta)$
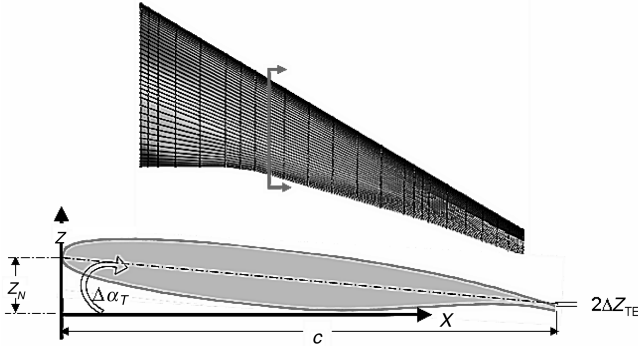local chord length $c(\eta)$

Fig. 33   Wing airfoil section.

nondimensional upper surface coordinate

$$\zeta_U(\eta) = \frac{z_U(\eta)}{c(\eta)}$$

nondimensional local wing shear

$$\zeta_N(\eta) = \frac{z_N(\eta)}{c(\eta)}$$

local wing twist angle $\alpha_T(\eta)$

Equation (20) is the equation for the wing upper surface; the similar equation for the lower surface is

$$\zeta_L(\psi, \eta) = \zeta_N(\eta) + C_{1.0}^{0.5}(\psi)S_L(\psi, \eta) + \psi[\zeta_T(\eta) - \tan\alpha_T(\eta)] \tag{36}$$

The physical z coordinate is transformed into the shape function using an extension of the airfoil shape function procedure to derive Eq. (2). The corresponding shape function for an airfoil section on a wing with vertical shear and local section twist is given by the equation

$$S_U(\psi, \eta) = \frac{\zeta_U(\psi, \eta) - \zeta_N(\eta) - \psi[\zeta_T(\eta) - \tan\alpha_T(\eta)]}{C_{1.0}^{0.5}(\psi)} \tag{37}$$

The corresponding shape function equation for the lower surface of a wing is

$$S_L(\psi, \eta) = \frac{\zeta_L(\psi, \eta) - \zeta_N(\eta) - \psi[\zeta_T(\eta) - \tan\alpha_T(\eta)]}{C_{1.0}^{0.5}(\psi)} \tag{38}$$

For a given wing definition, the wing upper and lower shape functions can be calculated using Eqs. (37) and (38).

Given a wing definition as a shape function surface in the design space, the wing upper and lower surfaces in physical space can be determined from the shape function surfaces, the local values of twist, shear, and local chord lengths as

$$
\begin{aligned}
z_U(x, y) &= \Big\{\zeta_N(\eta) + C_{1.0}^{0.5}(\psi, \eta)S_U(\psi, \eta) \\
&\quad + \psi[\zeta_T(\eta) - \tan\alpha_T(\eta)]\Big\}C_{\text{LOCAL}}(\eta) \\
z_L(x, y) &= \Big\{\zeta_N(\eta) + C_{1.0}^{0.5}(\psi, \eta)S_L(\psi, \eta) \\
&\quad + \psi[\zeta_T(\eta) - \tan\alpha_T(\eta)]\Big\}C_{\text{LOCAL}}(\eta)
\end{aligned}
\tag{39}
$$

Figure 34 illustrates the general process of transforming the shape function surfaces for a wing in the design space into the physical definition of the wing. The unit design space is defined by $\psi = 0.0–1.0$, and $\eta = 0.0–1.0$ and therefore represents any wing planform.

The class function exponents in Fig. 34 are shown to potentially vary with the spanwise station η. For a subsonic wing, the class function exponents are constant across the wing. However, a supersonic wing type planform often has a highly swept inboard
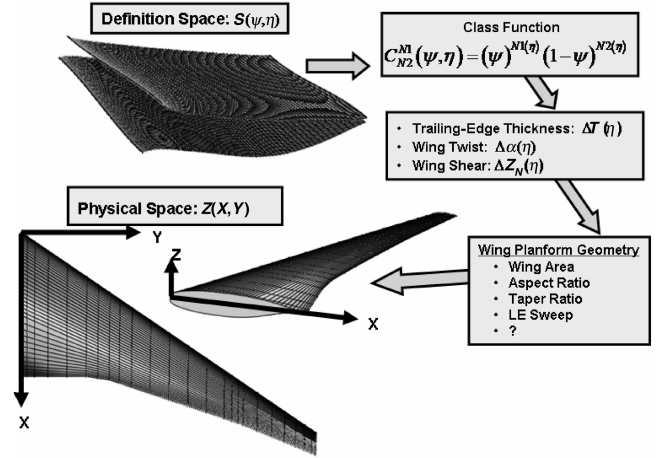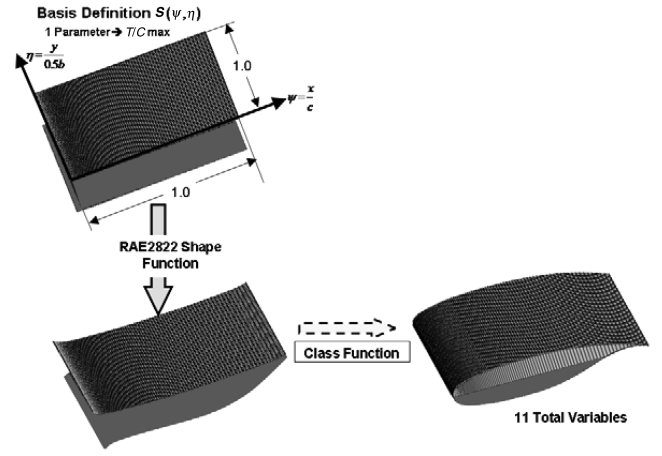

Fig. 34   Transformation from design space to physical space.

Fig. 35   Parametric wing design space, ψ, η, S.

panel with a subsonic round-nose leading edge, and a reduced sweep outboard supersonic leading-edge panel with shape nose airfoils. In this case, the class function for the outboard wing panel would be different than that on the inboard panel. Figures 35–38 show an example of process of transformation from the unit basis wing definition in the design space into a specific physical detailed wing definition. Figure 35 shows the wing section shape corresponding to a unit basis shape function surface and the effect of changing the unit shape function into the shape function corresponding to a constant RAE2822-type airfoil across the wing span. This would require, as shown in Fig. 10, about 11 variables to define the upper and lower surface of the airfoil. The effect of including a spanwise variation of maximum thickness ratio is shown in Fig. 36. This represents the complete wing definition in the ψ, η design space.
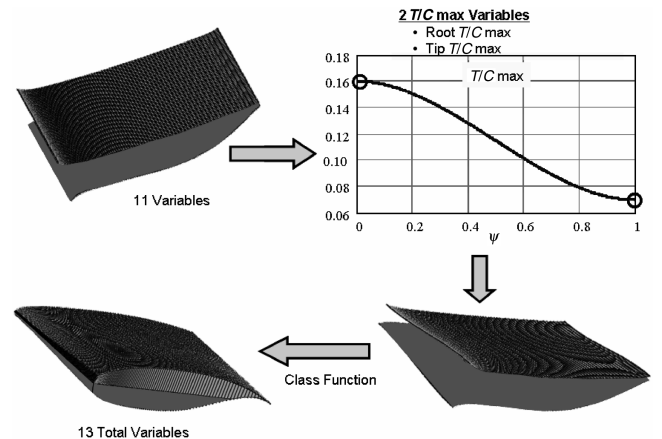

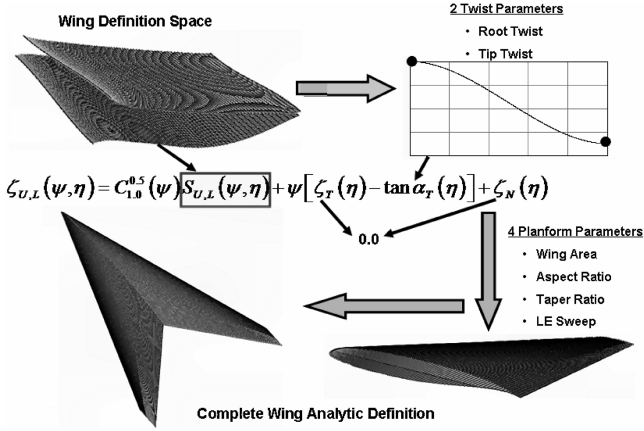**Fig. 36   Incorporate spanwise variation of wing thickness.**

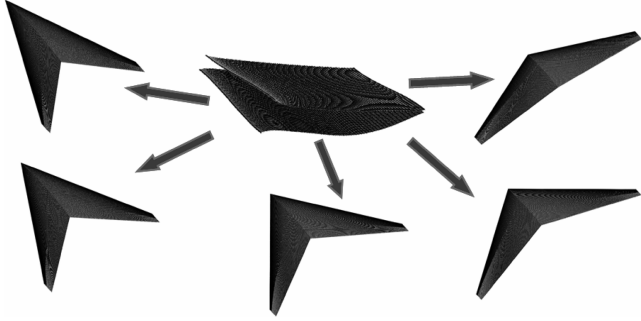**Fig. 37 Complete parametric wing definition.**

Fig. 38 Parametric wing definition: varied wing sweep.

Figure 37 shows transformation of the wing in design space into the complete physical wing definition. The key parameters that define the wing planform and the spanwise twist distribution are also shown.

In this example, the complete parametric cambered wing definition with spanwise variations of maximum thickness and wing twist, and specified wing area, sweep, aspect ratio, and taper ratio, required only a total of 19 design variables:

1) The supercritical airfoil section required 11 design variables.
2) The spanwise thickness variation required 2 variables.
3) The spanwise twist variation required 2 variables.
4) The wing area required 1 variable.
5) The aspect ratio required 1 variable.
6) The taper ratio required 1 variable.
7) The leading-edge sweep required 1 variable.

Figure 38 shows that the same design space definition of a wing can define detailed surface geometry for a variety of wing planforms depending on the planform defining parameters. In the cases shown, the various planforms are obtained by varying wing sweep while keeping the structural aspect ratio constant.

XII. Mathematical Description of a Wing in Design Space

Similar to the shape function for an airfoil, the shape function design surface for simple wings, such as shown in Fig. 38, is a smooth continuous analytic surface. Consequently, the shape function surface can be described by a Taylor series expansion in x and y. It is shown in [10] that a Taylor series expansion in x and y is equivalent to a Taylor series expansion in x with the each of the x coefficients then represented by a Taylor expansion in y.

Similarly, a power series in x and y is exactly equal to a power series in x with the x coefficients represented by power series expansions in y.

Therefore, the shape function surface for a complete wing surface can be obtained by first selecting the order of the Bernstein polynomial to represent the wing airfoils. The complete wing shape function surface can then be defined by expanding the coefficients of

the Bernstein polynomial in the spanwise direction using any appropriate numerical technique. The surface definition of the wing is then obtained by multiplying the shape function surface by the wing class function.

Physically, this means that the root airfoil is represented by a series of composite airfoils defined by the selected Bernstein polynomial. The entire wing is then represented by the same set of composite airfoils. The magnitude of each composite airfoil varies across the wing span according to the spanwise expansion technique and wing definition objectives. For example, the definition objective could be a constrained wing design optimization.

An example of the mathematical formulation of this process is shown next, using Bernstein polynomials to represent the streamwise airfoil shapes, as well as the spanwise variation of the streamwise coefficients.

The unit streamwise shape functions for Bernstein polynomial of order Nx are defined as

$$Sx_i(\psi) = Kx_i \psi^i (1 - \psi)^{Nx-i} \quad \text{for } i = 0\text{–}Nx \qquad (40)$$

where the streamwise binomial coefficient is defined as

$$Kx_i \equiv \binom{Nx}{i} \equiv \frac{Nx!}{i!(Nx-i)!} \qquad (41)$$

The streamwise upper surface shape function at the reference spanwise station η_{REF} is

$$Su(\psi, \eta_{\text{REF}}) = \sum_{i=1}^{Nx} Au_i(\eta_{\text{REF}}) Sx_i(\psi) \qquad (42)$$

Let us represent the spanwise variation of each of the coefficients $Au_i(\eta)$ by Bernstein polynomials as

$$Au_i(\eta) = \sum_{j=1}^{Ny} Bu_{i,j} Sy_j(\eta) \qquad (43)$$

where

$$Sy_j(\psi) = Ky_j \eta^j (1 - \eta)^{Ny-j} \quad \text{for } j = 0\text{–}Ny \qquad (44)$$

and

$$Ky_j \equiv \binom{Ny}{j} \equiv \frac{Ny!}{j!(Ny-j)!} \qquad (45)$$

The wing upper surface is then defined by

$$\zeta_U(\psi, \eta) = C_{N2}^{N1}(\psi) \sum_i^{Nx} \sum_j^{Ny} [Bu_{i,j} Sy_j(\eta) Sx_i]$$
$$+ \psi[\zeta_T(\eta) - \tan\alpha_{\text{TWIST}}(\eta)] + \zeta_N(\eta) \qquad (46)$$

The similar equation for the lower surface is

$$\zeta_L(\psi, \eta) = C_{N2}^{N1}(\psi) \sum_i^{Nx} \sum_j^{Ny} [Bl_{i,j} Sy_j(\eta) Sx_i]$$
$$+ \psi[\zeta_T(\eta) - \tan\alpha_{\text{TWIST}}(\eta)] + \zeta_N(\eta) \qquad (47)$$

In Eqs. (46) and (47), the coefficients $Bu_{i,j}$ and $Bl_{i,j}$ define the unique geometry of the wing upper and lower surfaces. In a design optimization study, the coefficients $Bu_{i,j}$ and $Bl_{i,j}$ would be the optimization variables.

Continuity of curvature from the upper surface around the leading edge to the lower surface is easily obtained by the requirement $Bu_{0,j} = Bl_{0,j}$.

The component shape function terms Sx_i represent the ith basic composite airfoil shapes. The terms Sy_i represent the jth spanwise distribution for any of the composite airfoils. Therefore, each product $Sx_i Sy_i$ defines one of the $(Nx + 1)(Ny + 1)$ composite wing shapes that are used to develop the total upper or lower surface definitions.
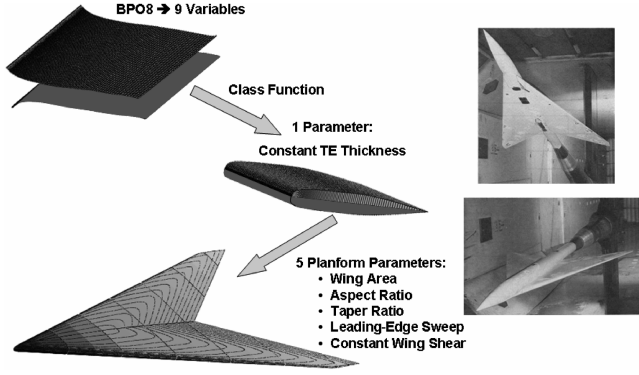
Fig. 39 Scalar loft of a highly swept aeroelastic loads wind-tunnel model.

The actual wing surface coordinates can be obtained from the equations

$$y = \frac{b}{2}\eta \qquad x = \psi C_{\text{LOC}}(\eta) + x_{\text{LE}}(\eta)$$

$$z_U(x,y) = \zeta_U(\psi,\eta) C_{\text{LOC}}(\eta) \qquad z_L(x,y) = \zeta_L(\psi,\eta) C_{\text{LOC}}(\eta)$$

$$(48)$$

This process of defining a wing geometry using Eqs. (46–48) may be considered a *scalar loft* of a wing where every point on the wing surface is defined as accurately as desired and the points are all "connected" by the analytic equations. This is in contrast to the usual wing definition as a *vector loft* which is defined as ordered sets of x, y, z coordinates plus "rules" that describe how to connect adjoining points. The common approach used to connect adjacent points is along constant span stations and along constant percent chord lines.

Figure 39 shows an example of a scalar loft of a highly swept wind-tunnel wing that was used to obtain surface pressure and wings loads data for CFD validation studies [13,14]. The model was built using the conventional vector loft approach.

The analytic scalar loft of the wing was defined by a total of 15 parameters. These included 1) BPO8 representation of the basic airfoil section (9 parameters), 2) wing area, 3) aspect ratio, 4) taper ratio, 5) leading-edge sweep, 6) trailing-edge thickness (constant across the span), and 7) constant wing shear (to fit the wing on the body as a low wing installation).

The differences between the analytic wing surface definition and the "as built" wing surface coordinates were well within the wind-tunnel model construction tolerances over the entire wing surfaces.

XIII. Mathematical Description of a Wing Having Leading-Edge and/or Trailing-Edge Breaks

Subsonic and supersonic transport aircraft wings typically have planform breaks in the leading edge (e.g., strake) and/or the trailing edge (e.g., yehudi) with discontinuous changes in sweep. Consequently, the wing surface is nonanalytic in the local region of the edge breaks. However, the approach of defining a complete wing geometry as previously described should be applicable. The airfoil sections across the wing can be defined by the composite set of component airfoils corresponding to the selected order of Bernstein polynomial representation. The spanwise variation of the composite airfoil scaling coefficients would be most likely piecewise continuous between planform breaks.

To explore this concept, the geometry of a typical subsonic aircraft wing was analyzed in depth. Airfoil sections at a large number of spanwise stations were approximated by equal order of Bernstein polynomial representation of the corresponding wing section airfoil shape functions. The adequacy of the composite representation was determined by computing the residual differences between the actual airfoil sections and those defined by the approximating Bernstein polynomials. The calculated shape function surfaces corresponding to wing upper and lower surfaces are shown in Fig. 40. The piecewise continuous nature of the surfaces associated with the planform
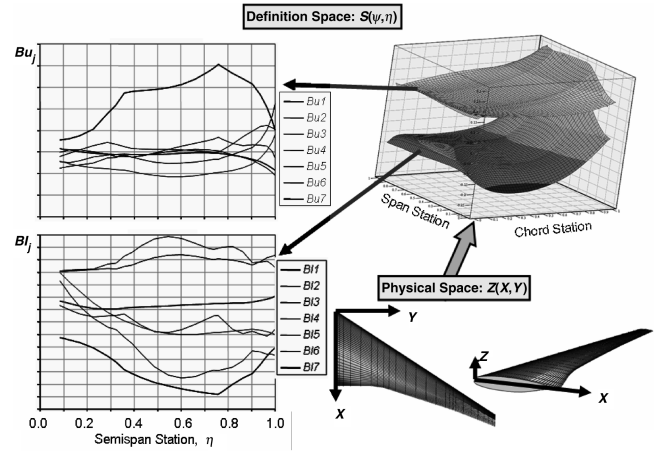

Fig. 40 Spanwise variation of the BP composite airfoil scaling coefficients.
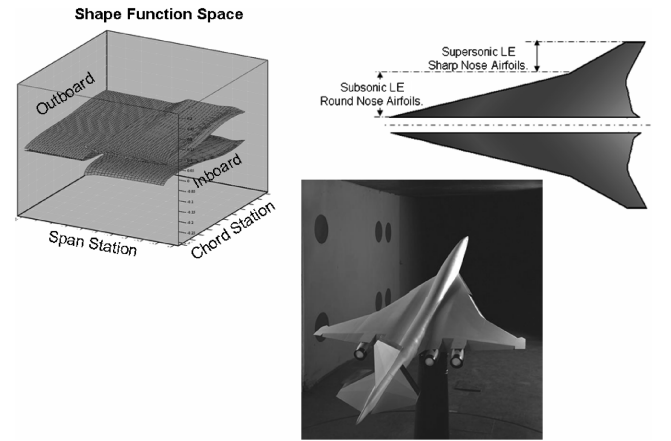

Fig. 41 Shape function for an HSCT supersonic wing.

breaks is very evident. The corresponding spanwise variations of the composite airfoil computed scaling coefficients Bu_j and Bl_j are also shown.

These results show that the spanwise variations of the Bernstein coefficients across the wing span are very regular, piecewise continuous, and well behaved.

The shape function surfaces for a typical high-speed civil transport (HSCT) wing are shown in Fig. 41. This planform has a number of leading-edge and trailing-edge breaks. This wing has an inboard subsonic leading-edge wing with round-nose airfoils. Outboard of the leading edge, the wing has a supersonic leading edge with sharp nose airfoils. The shape functions for this wing are also seen to be piecewise smooth and continuous.

The results shown in Figs. 37–41 indicate that the concept of a scalar wing definition is indeed a viable and promising wing definition methodology.

XIV. Summary and Conclusions

The class function/shape function transformation (CST) geometry representation method is a unique and powerful new geometry representation method. The class function defines fundamental classes of airfoils, axisymmetric bodies, and axisymmetric nacelles geometries. The shape function defines unique geometric shapes within each fundamental class.

The mathematical simplicity of using the shape function for geometry representation is readily apparent in applications to airfoils or wing geometries with round-nose geometries. The shape function eliminates the numerical leading-edge singularities in slopes, second derivatives, and the large variations in curvature over the entire surface of the geometry. In addition, the shape function provides direct control of key design parameters such as leading-edge radius,

continuous curvature around a leading edge, boat-tail angle, and closure to a specified thickness.

The use of Bernstein polynomials is an attractive and systematic technique to decompose the basic unit shape into scalable elements corresponding to discrete component airfoils. This technique 1) captures the entire design space of smooth airfoils, axisymmetric bodies, and nacelles; and 2) within this design space, all smooth airfoils, axisymmetric bodies, and nacelles are derivable from the unit shape function and therefore from each other.

The class function/shape function transformation geometry representation methodology can be used to describe both the cross-sectional shapes of arbitrary bodies or nacelles, as well as the distribution of the cross section shapes along the primary body axis. The examples shown in the paper illustrated the versatility of the methodology in that only a few design variables are required to define detailed definitions of the external shape and inlet geometry of a nonsymmetric nacelle.

The concept of "analytic scalar definitions of composite wing surfaces" was introduced and explored. With this approach, the wing airfoil shapes functions are represented by a Bernstein polynomial. The selected order of Bernstein polynomial effectively defines a set of composite airfoils for constructing the wing surface definitions. The coefficients of the Bernstein polynomials can then be mathematically expanded in the spanwise direction to define the complete wing upper and lower shape function surfaces. The shape function surfaces are then easily transformed into the physical wing geometry as composite wing shapes that can be used for design optimization and parametric design studies.

The analytic CST geometry representation methodology presented in this report provides a unified and systematic approach to represent a wide variety of two-dimensional and three-dimensional geometries encompassing a very large design space with a relatively few scalar parameters.

References

[1] Sobieczky, H., "Aerodynamic Design and Optimization Tools Accelerated by Parametric Geometry Preprocessing," *European Congress on Computational Methods in Applied Sciences and Engineering*, ECCOMAS, 2000.

[2] Sobieczky, H., *Parametric Airfoils and Wings*, Notes on Numerical Fluid Mechanics, Vol. 68, Vieweg, Brunswick, Germany, 1998, pp. 71–88.

[3] Samareh, J. A., "Survey of Shape Parameterization Techniques for High-Fidelity Multidisciplinary Shape Optimization," *AIAA Journal*, Vol. 39, No. 5, May 2002, pp. 877–884.

[4] Robinson, G. M., and Keane, A. J., "Concise Orthogonal Representation of Supercritical Airfoils," *Journal of Aircraft*, Vol. 38, No. 3, March 2001, pp. 580–583.

[5] Song, W., and Keane, A. J., "A Study of Shape Parameterization Airfoil Optimization," *10th AIAA/ISSMO Multidisciplinary Analysis and Optimization Conference*, AIAA Paper 2004-4482, 2004.

[6] Padula, S., and Li, W., "Options for Robust Airfoil Optimization Under Uncertainty," *9th AIAA Multidisciplinary Analysis and Optimization Symposium*, AIAA Paper 2002-5602, 2002.

[7] Hicks, R. M., and Henne, P. A., "Wing Design by Numerical Optimization," *Journal of Aircraft*, Vol. 15, No. 7, 1978, pp. 407–412.

[8] Samareh, J. A., "Aerodynamic Shape Optimization Based on Free-Form Deformation," AIAA 2004-4630, Sept. 2004.

[9] Kulfan, B. M., and Bussoletti, J. E., "Fundamental Parametric Geometry Representations for Aircraft Component Shapes," *11th AIAA/ISSMO Multidisciplinary Analysis and Optimization Conference: The Modeling and Simulation Frontier for Multidisciplinary Design Optimization*, AIAA Paper 2006-6948, 2006.

[10] Kulfan, B. M., "Universal Parametric Geometry Representation Method: "CST"," *45th AIAA Aerospace Sciences Meeting and Exhibit*, AIAA Paper 2007-0062, Jan. 2007.

[11] Timothy, W., Purcell, T. W., and Om, D., "TRANAIR Packaging for Ease-of-Use in Wing Design," *AIAA and SAE 1998 World Aviation Conference*, AIAA Paper 1998-5575, Sept. 1998.

[12] Samant, S. S., Bussoletti, J. E., Johnson, F. T., Burkhart, R. H., Everson, B. L., Melvin, R. G., Young, D. P., Erickson, L. L., and Madson, M. D., "TRANAIR: A Computer Code for Transonic Analyses of Arbitrary Configurations," *Aerospace Sciences Meeting, 25th*, AIAA Paper 1987-34, Jan. 1987.

[13] Manro, M. E., Percy, J., Bobbitt, P. J., and Kulfan, R. M., "The Prediction of Pressure Distributions on an Arrow Wing Configuration Including the Effects of Camber Twist and a Wing Fin," NASA -2108 Paper No. 3, Nov. 1979, pp. 59–115.

[14] Wery, A. C., and Kulfan, R. M., "Aeroelastic Loads Prediction for an Arrow Wing: Task 2 Evaluation of Semi-Empirical Methods," NASA CR-3641, March 1983.